Hindawi
Journal of Spectroscopy
Volume 2022, Article ID 7019037, 11 pages
https://doi.org/10.1155/2022/7019037

Research Article

Nano-Polyoxotungstate $[Cu_{20}P_8W_{48}]$ Immobilized on Magnetic Nanoparticles as an Excellent Heterogeneous Catalyst Nanoreactors for Green Reduction of Nitrophenol Compounds

Reza Haddad[1] **and Ali Roostaie**[2]

[1]*Inorganic Chemistry, Department of Police Equipment and Technologies, Policing Sciences and Social Studies Institute, Tehran, Iran*
[2]*Analytical Chemistry, Department of Police Equipment and Technologies, Policing Sciences and Social Studies Institute, Tehran, Iran*

Correspondence should be addressed to Reza Haddad; haddad.reza2009@yahoo.com

Received 21 November 2021; Accepted 19 April 2022; Published 26 May 2022

Academic Editor: Pedro D. Vaz

In this study, Cu_{20}-polyoxotungstate $[Cu_{20}Cl(OH)_{24}(H_2O)_{12}(P_8W_{48}O_{184})]^{25-}$ supported on a magnetic substrate was used as a high-performance green method for the reduction of nitrophenol compounds such as 4-nitrophenol (4-NP) and 2,4,6-trinitrophenol (2,4,6-TNP). $[Fe_3O_4@SiO_2\text{-}NH_2\text{-}Cu_{20}P_8W_{48}]$ as heterogeneous magnetic nanocatalyst was synthesized and characterized by FT-IR, SEM, TEM, VSM, and TGA. This nanocatalyst has an excellent efficiency in the reduction of nitrophenol compounds to aminophenol compounds. The UV-Vis absorption spectrum is used at different times to evaluate the progress of the reaction. Under optimal conditions, 100% conversion and selectivity in reduction of 4-NP and 2,4,6-TNP to 4-AP and 2,4,6-TAP were obtained, respectively. In addition, after the reaction, the $[Fe_3O_4@SiO_2\text{-}NH_2\text{-}Cu_{20}P_8W_{48}]$ was recovered using an external magnetic field and used for the next cycle. The results showed that the nanocatalyst can perform eight consecutive cycles without any significant decrease in efficiency. In the end, according to the results, the proposed mechanism for this reaction was reported.

1. Introduction

Today, the world is facing an increasing population growth and consequently an increase in pollutants. Many research groups are working to solve environmental problems and remove pollutants from the environment and provide the best and safest way to obtain the desired products without causing any pollution to nature.

Nanocatalysts as part of the science of nanotechnology to the global market have been able to occupy a large part of this market. Nanocatalysts have been able to overcome many of the challenges in catalysts by having active sites with a core of metal atoms, metal ions, and creating holes around the sites [1–3]. A special group of organic compounds whose treatment from industrial effluents is one of the main concerns due to its toxicity and hazard is phenols and phenolic compounds. These substances are hydroxyl benzene derivatives that may occur in industrial and domestic effluents. The main sources of phenol pollution in the aquatic environment include wastewater from the paint industry, pesticides, coal conversion industry, polymer resin, and oil and petrochemical industries. One of the most common pollutants in industrial and agricultural effluents is 4-nitrophenol, which causes serious damage to the environment and the body of animals. The presence of these pollutants, in addition to irreversible effects on the ecosystem and causing aesthetic problems, has also had adverse effects such as mutagenesis and cancer in living organisms [4]. Nitrophenols are very harmful to both nature and humans due to their toxicity and carcinogenicity and are

known as one of the largest high-risk pollutants, and various researches have been done to reduce and eliminate them [5]. This material is highly resistant to degradation and natural decomposition processes.

However, these compounds can be converted to less toxic aminophenol compounds that are used as intermediates in the production of pharmaceuticals, cosmetics, agrochemicals, dyes, and polymers [6].

Therefore, it is necessary to think of a way to eliminate it. Removal of 4-nitrophenol by conventional methods is very slow and therefore time-consuming. A strong catalyst can help remove this contaminant and other nitro-aromatic compounds. There are several different methods for reducing these compounds to the corresponding amines, including hydrogenation with the help of intermediate metals and hydrogen gas, electrochemical reduction, and reduction by hydrazine. But one of the most important methods is the catalytic reduction of nitroaromatic compounds to their corresponding amino aromatic compounds.

However, the chemical reduction reaction of nitrophenol compounds is very slow and the use of a suitable catalyst is essential for the development of this method. Among the various types of nanocatalysts, nano-polyoxometalates (Nano-POM) have attracted the attention of researchers due to their many applications in various fields. Nano-POMs also have a special place in industrial and laboratory processes. Due to the importance of Nano-POMs in recent years as electron transfer catalysts and solid catalysts in various reactions and countless other applications of these compounds, the interest in using these compounds as catalysts has increased greatly. The importance of polyoxometalates became apparent in the mid-nineteenth century with the recognition of their functional properties, and gradually with the complete knowledge of their properties and applications, the value of these compounds was increased. The structural diversity of polyoxometalates gives them interesting properties in the fields of catalytic [7], pharmaceutical [8], electrochemistry [9], separation [10], gas adsorption [11], and sensors [12]. Due to the high negative charge and surface water molecules in polyoxometalates, these compounds have high solubility in polar solvents and are hydrophilic [13]. On the other hand, because the accumulation of Nano-POM is inevitable; therefore, the use of an ideal preservative to reduce the accumulation and solubility of these compounds is essential. To prevent the accumulation and thus overcome the problems of stability, separation, and recovery of polyoxometalates, various substrates such as zeolite [14], graphene oxide [15], TiO_2 [16], and Fe_3O_4 [17] have been used as a preservative for these compounds. Among these, Fe_3O_4 NPs, because of the low cost of synthesis, environmental compatibility, and electronic-optical properties, have been widely used as an effective substrate for immobilizing many catalysts. Various reports have been reported about the reduction of nitrophenol compounds with different types of polyoxometalates under different conditions. For example in 2012, Parida and Rana using immobilizing of Keggin type of phosphotungstate on MCM-41 (LPdW/MCM-41) were able to reduction of the 4-nitrophenol with 99% conversion and 100% selectivity to 4-aminophenol [18]. Manganese-substituted polyoxomolybdate supported on silver nanoparticles has been reported by Lan et al. to reduction of the 4-nitrophenol. However, by removing silver nanoparticles from the POM surface, a 50% decrease in activity was observed [19]. In the present paper, to prevent self-aggregation of wheel-shaped polyoxotungstate $[Cu_{20}Cl(OH)_{24}(H_2O)_{12}(P_8W_{48}O_{184})]^{25-}$ and also easier recovery for use in subsequent reaction cycles, $[Cu_{20}Cl(OH)_{24}(H_2O)_{12}(P_8W_{48}O_{184})]^{25-}$ supported on the magnetic substrate $[Fe_3O_4@SiO_2\text{-}NH_2]$ by electrostatic interactions between the cationized support and the $[Cu_{20}P_8W_{48}]$ anion [20, 21]. The catalytic activity of nanocomposite $[Fe_3O_4@SiO_2\text{-}NH_2\text{-}Cu_{20}P_8W_{48}]$ as a recyclable and effective catalyst in the reduction of 4-NP and 2,4,6-TNP in the presence of water as the most abundant and cheapest solvent compared to other solvents, which played a vital role in the development of "green" chemistry, was investigated (Scheme 1). The results showed 100% conversion and selectivity in the conversion of nitrophenol compounds to aminophenol compounds.

2. Experimental Section

2.1. Materials. 4-nitrophenol, 2,4,6-trinitrophenol, $FeCl_2.4H_2O$, $FeCl_3.6H_2O$, hydrochloric acid, ethanol, toluene, $CuCl_2{\cdot}2H_2O$, and $LiCH_3COO$ were purchased commercially from Sigma-Aldrich Co. Sodium borohydride ($NaBH_4$), tetraethyl orthosilicate (TEOS), and (3-aminopropyl)triethoxysilane were purchased from Merck Co.

2.2. Apparatus for Characterization. Analyses of the reaction products were conducted using a gas chromatograph (GC). PerkinElmer 780 instrument was used to record the FT-IR spectrum. TEM images were recorded using the model Philips CM 10 device. SEM images were also obtained using the Model XL-30 FEG SEM, Philips, at 20 kV by SEM instrumentation. TGA (Shimadzu 50) and VSM (7404 USA) techniques were also used to identify the nanocatalyst.

2.3. Methods

2.3.1. Synthesis of $[Fe_3O_4]$ Nanoparticles. Add 5.40 g of $FeCl_2.4H_2O$ and 2 g of $FeCl_3.6H_2O$ to 25 mL of an aqueous solution of 2 M hydrochloric acid at room temperature and stir until the salts are completely dissolved. Then, 40 mL of aqueous ammonia solution (25%) was slowly added to the reaction mixture at room temperature for 20 min under an argon atmosphere and stirred for about 30 minutes with a mechanical stirrer. Finally, the $[Fe_3O_4]$ NPs are separated by an external magnet and washed three times with deionized water and ethanol, and dried in vacuum.

2.3.2. Synthesis of $[Fe_3O_4@SiO_2]$ Core-Shell. To synthesize $[Fe_3O_4@SiO_2]$ core-shell nanoparticles, add 35 mL of ethanol and 6 mL of deionized water to the iron nanoparticles synthesized from the previous step and sonicate for 15 min.

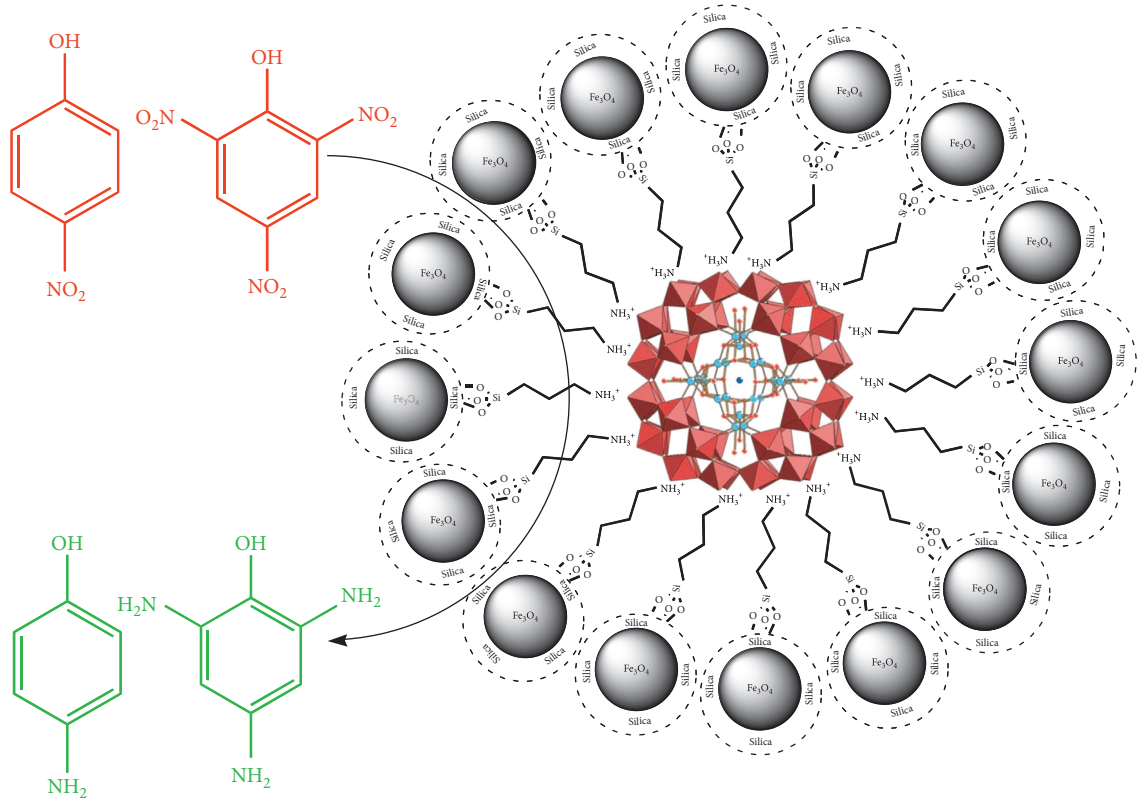

Scheme 1: Reduction of nitrophenol compounds with $[Fe_3O_4@SiO_2\text{-}NH_2\text{-}Cu_{20}P_8W_{48}]$.

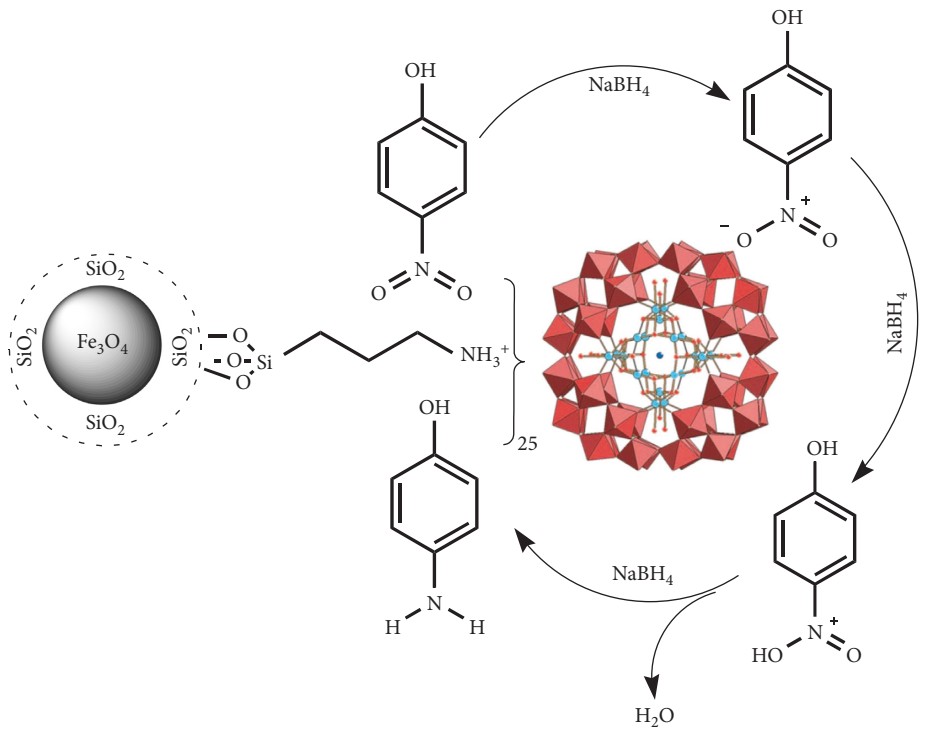

Scheme 2: A plausible mechanism for the reduction of 4-NP and 2,4,6-TNP to aminophenol compounds in the presence of $[Fe_3O_4@SiO_2\text{-}NH_2\text{-}Cu_{20}P_8W_{48}]$ nanocatalyst and $NaBH_4$.

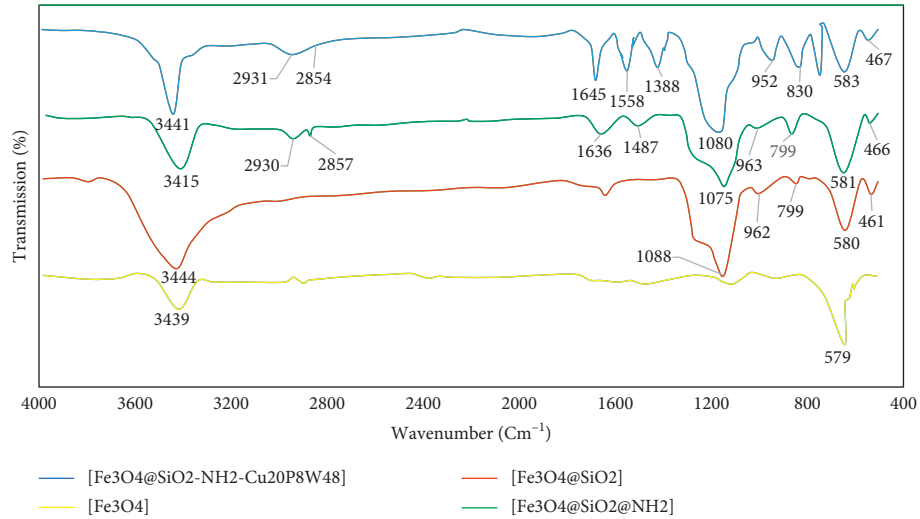

FIGURE 1: FT-IR spectrum of $[Fe_3O_4]$, $[Fe_3O_4@SiO_2]$, $[Fe_3O_4@SiO_2\text{-}NH_2]$, and $[Fe_3O_4@SiO_2\text{-}NH_2\text{-}Cu_{20}P_8W_{48}]$.

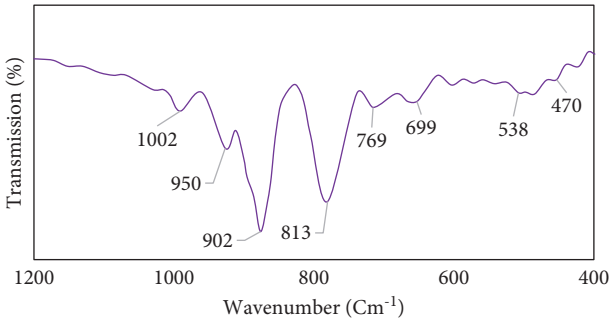

FIGURE 2: FT-IR spectrum of $[Cu_{20}Cl(OH)_{24}(H_2O)_{12}(P_8W_{48}O_{184})]^{25-}$.

Then, slowly add 1.5 mL of tetraethyl orthosilicate (TEOS) to this solution and sonicate again for about 10 min. In the next step, 1.40 mL of aqueous ammonia solution (10%) is added and subjected to mechanical stirrer for 10 min. The reaction mixture is placed at 40°C for about 12 h, and then, the magnetic nanoparticles are separated using an external magnet and washed several times with water and ethanol and dried in vacuum.

2.3.3. Synthesis of $[Fe_3O_4@SiO_2\text{-}NH_2]$. To 10 g of $[Fe_3O_4@SiO_2]$ nanoparticles, add 200 mL of toluene and sonicate for 30 min, then add 2.50 mL (3-aminopropyl) triethoxysilane (APTS) under mechanical stirring and mix gently until it is heated at 105°C for 20 h. The sample $[Fe_3O_4@SiO_2\text{-}NH_2]$ is then separated by an external magnet and washed three times with water and ethanol and dried in vacuum.

2.3.4. Preparation of $[Cu_{20}Cl(OH)_{24}(H_2O)_{12}(P_8W_{48}O_{184})]^{25-}$. To 20 mL of 1 M buffer solution of $LiCH_3COO$ at pH 6, add 0.1 g (0.6 mmol) $CuCl_2.2H_2O$, then 0.37 g (0.025 mmol) of $K_{28}Li_5[H_7P_8W_{48}O_{184}]\cdot 92H_2O$ (synthesized according to Ref. [43]). The reaction mixture is placed at 80°C for 1 h and filtered after cooling. The mother liquor is placed in an open beaker at room temperature, where after 1-2 days, the blue crystals appear due to the evaporation of the solvent. The crystals are collected and dried at room temperature [22, 23].

2.3.5. Synthesis of Heterogeneous Nanocatalyst $[Fe_3O_4@SiO_2\text{-}NH_2\text{-}Cu_{20}P_8W_{48}]$. 0.25 g of $[Fe_3O_4@SiO_2\text{-}NH_2]$ is mixed in 100 mL of water and then subjected to ultrasound for 1 h to form a dispersion mixture. After creating a dispersion mixture, add 10 mg $[Cu_{20}Cl(OH)_{24}(H_2O)_{12}(P_8W_{48}O_{184})]^{-25}$ and heat the mixture for 4 h at 95°C. Finally, the mixture is filtered and washed three times with water and ethanol.

2.3.6. Reduction of Nitrophenol Compounds. To a sample of 25 mL of an aqueous solution of 4-NP or 2,4,6-TNP with a concentration of 1 mM, 25 mL of freshly prepared $NaBH_4$ solution with a concentration of 0.1 M and 0.01 g of $[Fe_3O_4@SiO_2\text{-}NH_2\text{-}Cu_{20}P_8W_{48}]$ nanocatalyst was added and stirred at room temperature. Monitor the progress of the reaction by diluting 1 mL of the reaction solution to 10 ml using the UV-Vis spectrum at regular intervals. The nanocatalyst is recovered in 8 successive steps. To perform the reduction reaction, 2,4,6-TNP using the same method as 4-NP was used.

3. Results and Discussion

3.1. Characterization of $[Fe_3O_4@SiO_2\text{-}NH_2\text{-}Cu_{20}P_8W_{48}]$

3.1.1. FT-IR Analysis. The FT-IR spectra of $[Fe_3O_4]$, $[Fe_3O_4@SiO_2]$, $[Fe_3O_4@SiO_2\text{-}NH_2]$, and $[Fe_3O_4@SiO_2\text{-}NH_2\text{-}Cu_{20}P_8W_{48}]$ are given in Figure 1. For the $[Fe_3O_4]$ NPs, the characteristic absorption peaks at 579 cm^{-1} are attributed to the Fe-O vibrations. However, the strong band

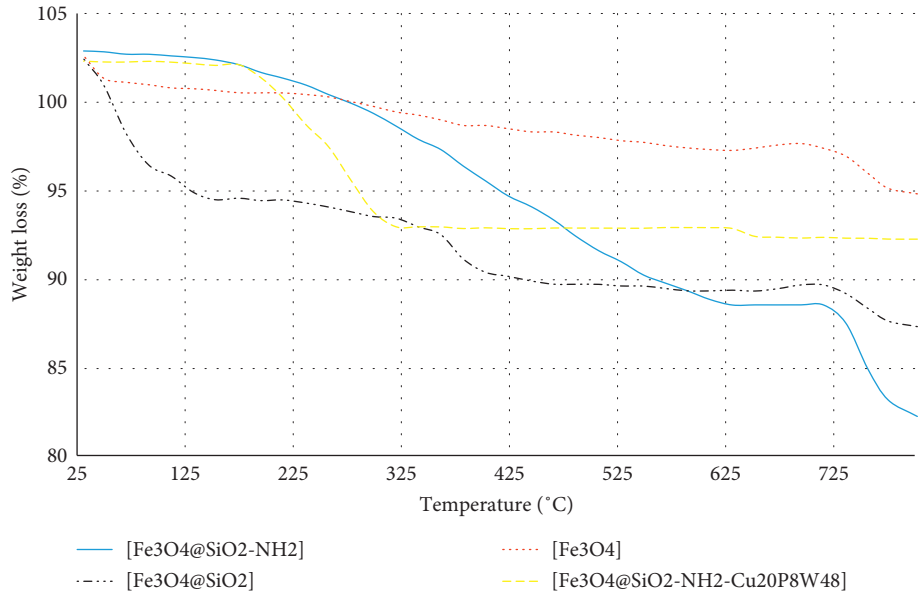

Figure 3: TGA of $[Fe_3O_4]$, $[Fe_3O_4@SiO_2]$, $[Fe_3O_4@SiO_2\text{-}NH_2]$, and $[Fe_3O_4@SiO_2\text{-}NH_2\text{-}Cu_{20}P_8W_{48}]$.

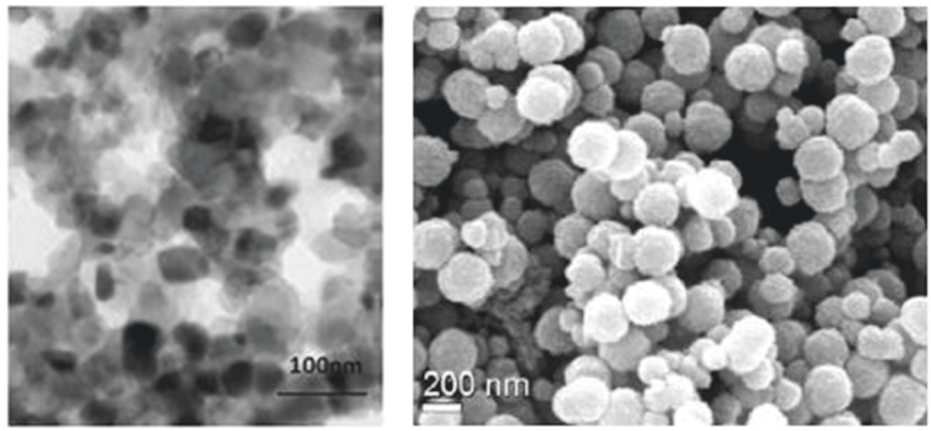

Figure 4: TEM (a) and SEM (b) images of $[Fe_3O_4@SiO_2\text{-}NH_2\text{-}Cu_{20}P_8W_{48}]$.

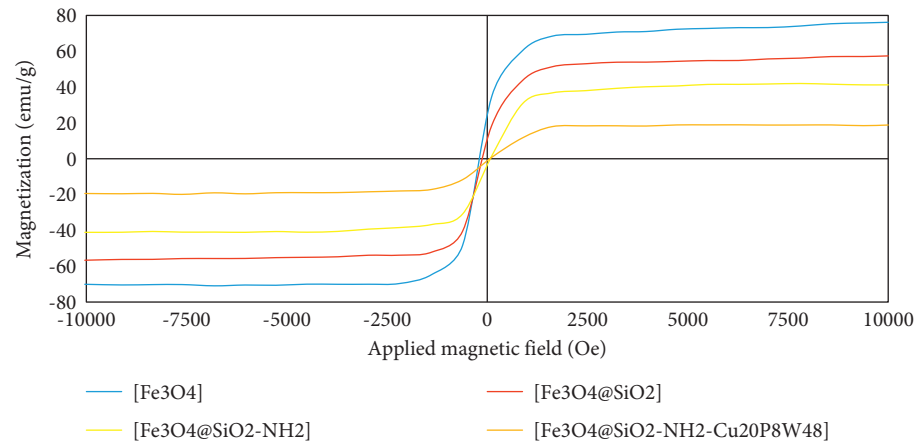

Figure 5: VSM test results for $[Fe_3O_4]$, $[Fe_3O_4@SiO_2]$, $[Fe_3O_4@SiO_2\text{-}NH_2]$, and $[Fe_3O_4@SiO_2\text{-}NH_2\text{-}Cu_{20}P_8W_{48}]$.

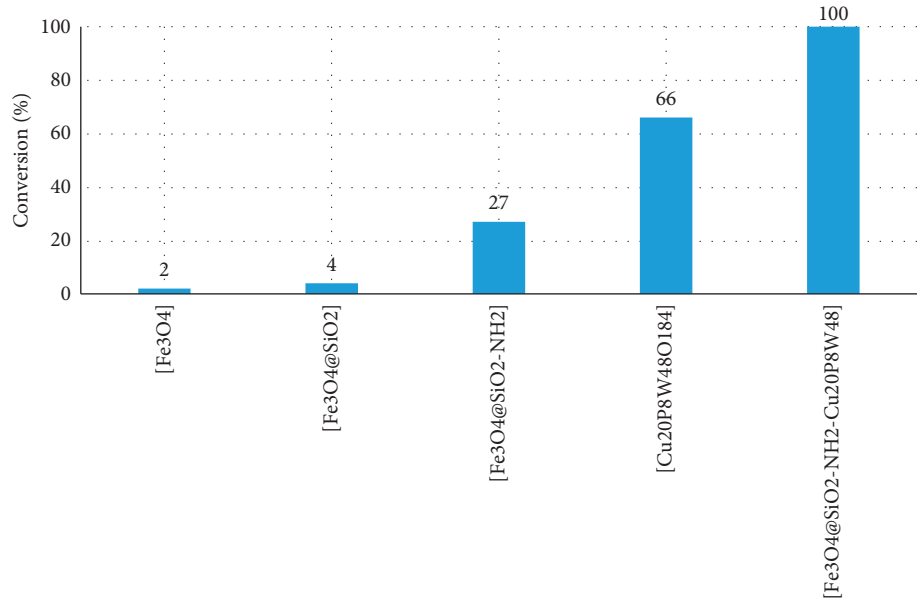

Figure 6: Comparison of the activity of $[Fe_3O_4@SiO_2\text{-}NH_2\text{-}Cu_{20}P_8W_{48}]$ catalyst and its components in reducing 4-NP.

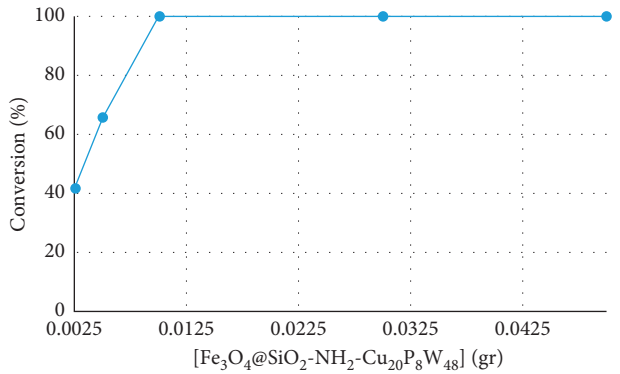

Figure 7: The effect of different amounts of nanocatalyst on the reduction of 4-NP.

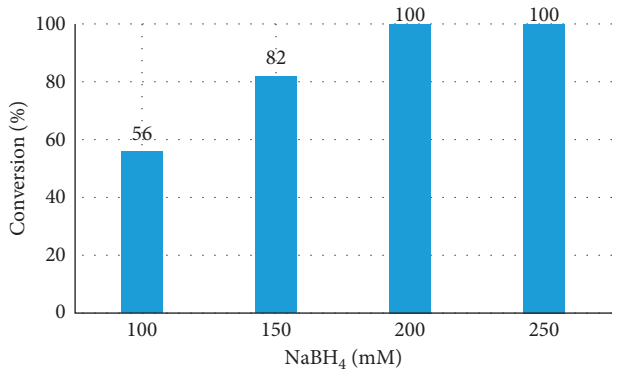

Figure 8: The effect of different amounts of $NaBH_4$ on the reduction of 4-NP.

at 3439 cm^{-1} is related to the stretching vibrations of Fe-OH groups. In the FT-IR spectrum of $[Fe_3O_4@SiO_2]$, three peaks are found in the 3400, 1088, and 799 cm^{-1} areas. The peak in region 3400 cm^{-1} corresponds to the hydrogen bond between Si-OH and water molecules on the surface. The peak in region 1088 cm^{-1} is related to unsymmetric stretching vibration siloxane bonding (Si-O-Si), and finally, the peak in region 799 cm^{-1} is related to symmetric stretching vibrations of Si-O-Si groups. Peaks related to the bending vibrations of Si-O-Si and Si-OH appear at 461 and 962 cm^{-1}, respectively. These peaks confirm the presence of a silica layer on the $[Fe_3O_4]$ nanoparticles. In $[Fe_3O_4@SiO_2\text{-}NH_2]$ FT-IR spectrum9 two new peaks are observed in the 2857 and 2930cm^{-1} regions related to the symmetric and the asymmetric stretching modes of the (-C-H) groups. In addition, the bending and stretching peaks of the amine group ($-NH_2$) appear in 1636 and 3415 cm^{-1}, respectively. The $-CH_2$ and $-CH_3$ groups (bending mode) also appear in the 1487 and 1388 cm^{-1} region, respectively. C-N stretching vibrations also appear at 1335 cm^{-1}. The N-H vibration peak appears at 1558 cm^{-1}. The FT-IR spectrum of $[Fe_3O_4@SiO_2\text{-}NH_2\text{-}Cu_{20}P_8W_{48}]$ nanocatalysts indicates the presence of $[Cu_{20}Cl(OH)_{24}(H_2O)_{12}(P_8W_{48}O_{184})]^{25-}$ in the magnetic substrate, which confirms the good interaction between $[Cu_{20}Cl(OH)_{24}(H_2O)_{12}(P_8W_{48}O_{184})]^{25-}$ and the magnetic substrate. According to the obtained results and FT-IR spectrum of $[Cu_{20}Cl(OH)_{24}(H_2O)_{12}(P_8W_{48}O_{184})]^{25-}$ (Figure 2), polyoxotungstate anions are stabilized on the surface of magnetic nanoparticles without changing the structure. The results of the FT-IR spectrum confirm this claim.

3.1.2. TGA. The thermal stability of $[Fe_3O_4]$, $[Fe_3O_4@SiO_2]$, $[Fe_3O_4@SiO_2\text{-}NH_2]$, and $[Fe_3O_4@SiO_2\text{-}NH_2\text{-}Cu_{20}P_8W_{48}]$ was investigated using the TGA method. According to Figure 3 in the case of $[Fe_3O_4@SiO_2]$, the first weight loss below 130°C is related to water evaporation (8.3%), and the second weight loss in the range of 130 to about 400°C is

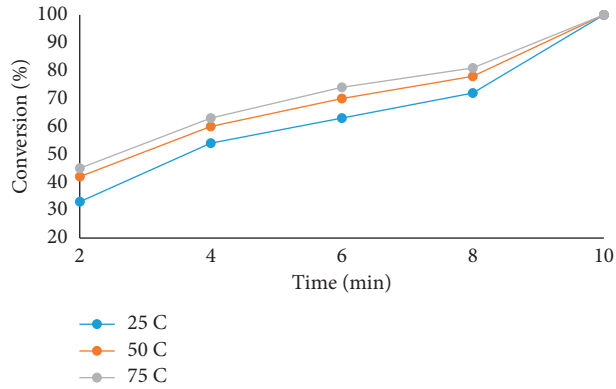

Figure 9: Reduction of 4-NP using various temperatures and times.

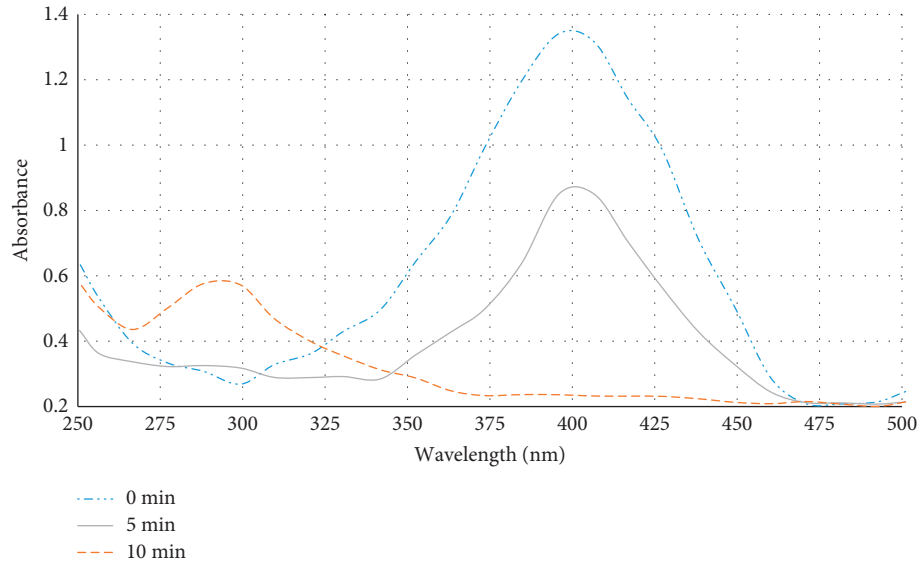

Figure 10: UV-Vis spectrum of an aqueous solution of 4-NP in the presence of 200 mM $NaBH_4$ and 0.01 g of [Fe_3O_4@SiO_2-NH_2-$Cu_{20}P_8W_{48}$].

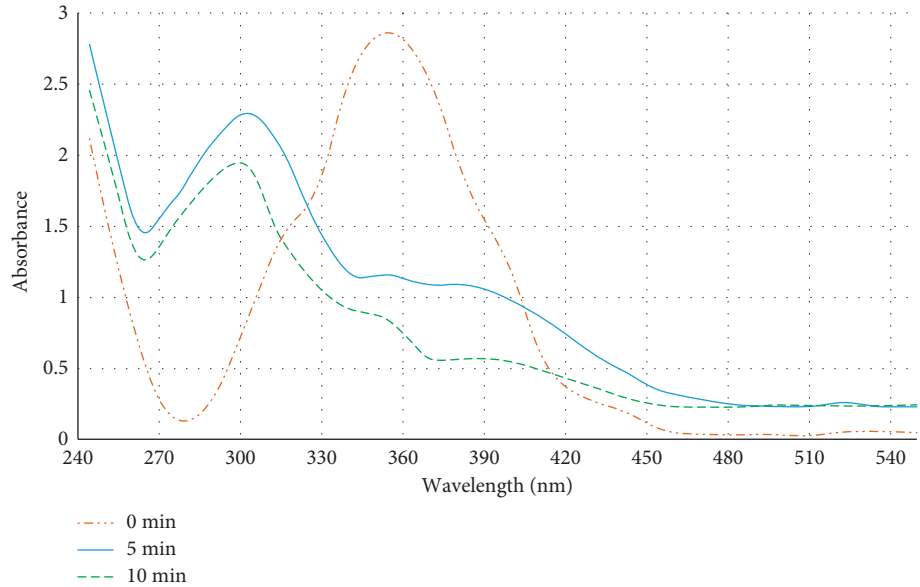

Figure 11: UV-Vis spectrum of an aqueous solution of 2,4,6-TNP in the presence of 200 mM $NaBH_4$ and 0.01 g of [Fe_3O_4@SiO_2-NH_2-$Cu_{20}P_8W_{48}$].

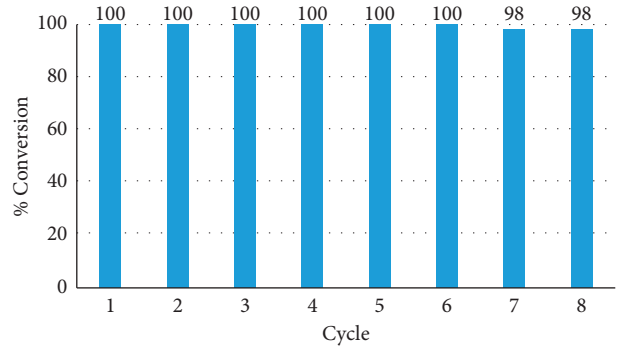

Figure 12: Reuse of $[Fe_3O_4@SiO_2\text{-}NH_2\text{-}Cu_{20}P_8W_{48}]$ for the reduction of 4-NP.

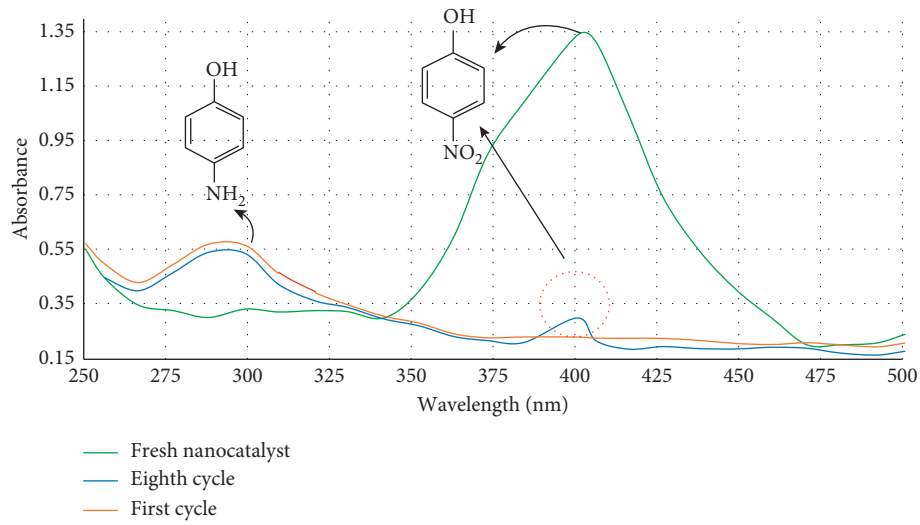

Figure 13: Comparison of UV-Vis spectra of the first and eighth cycles in the reduction of 4-NP by $[Fe_3O_4@SiO_2\text{-}NH_2\text{-}Cu_{20}P_8W_{48}]$.

related to physisorption molecules (4.2%). In the case of $[Fe_3O_4@SiO_2\text{-}NH_2]$, a weight loss of approximately 10.8% is observed in the temperature range of 230 to 625°C degrees due to the decomposition of the (3-aminopropyl) triethoxysilane (APS) groups. The decomposition of the $[Fe_3O_4@SiO_2\text{-}NH_2\text{-}Cu_{20}P_8W_{48}]$ was started at 200°C and was completely decomposed between 250 and 400°C, indicating the higher thermal stability of the catalyst. According to the TGA, the amount of $[Cu_{20}Cl(OH)_{24}(H_2O)_{12}(P_8W_{48}O_{184})]^{25-}$ is evaluated to be 6.8wt.%.

3.1.3. SEM and TEM Analysis. The SEM image of the heterogeneous nanocatalyst $[Fe_3O_4@SiO_2\text{-}NH_2\text{-}Cu_{20}P_8W_{48}]$ confirmed the uniformity and spherical morphology of the nanoparticles (Figure 4(b)). The average size of nanoparticles is in the range of 70–100 nm. Figure 4(a) shows the transmission electron microscopy (TEM) image of the $[Fe_3O_4@SiO_2\text{-}NH_2\text{-}Cu_{20}P_8W_{48}]$, which further confirmed an assembly of the catalyst and its size being less than 14 nm. The core-shell structure in magnetic nanoparticles with silica layer is clearly shown in Figure 4(a), which confirms the preservation of the morphology of nanoparticles after grafting with (3-aminopropyl) triethoxysilane.

3.1.4. VSM Analysis. To measure the magnetism of the synthesized samples, the test was performed at 25°C, and the corresponding hysteresis loops were prepared by changing the magnetic field H between +12000 and −12000 Oersted. According to Figure 5, the magnetic saturation was observed for $[Fe_3O_4]$, $[Fe_3O_4@SiO_2]$, $[Fe_3O_4@SiO_2\text{-}NH_2]$, and $[Fe_3O_4@SiO_2\text{-}NH_2\text{-}Cu_{20}P_8W_{48}]$ 52 emu/g, 38 emu/g, 27 emu/g, and 18 emu/g, respectively. According to the obtained values, the decreasing trend of magnetic saturation is due to the placement of SiO_2, alkylating agent, and $[Cu_{20}P_8W_{48}]$ nanocatalyst on $[Fe_3O_4]$ NPs. Remanent magnetization and negligible coercivity (Hc) in the results also indicate that the magnetic nanoparticles are superparamagnetic in all samples, which is fully established by converting the hysteresis ring to an S-shaped curve. It should be noted that the superparamagnetic behavior shown by these samples means that it is due to the reduction of particle size to the nanoparticle level.

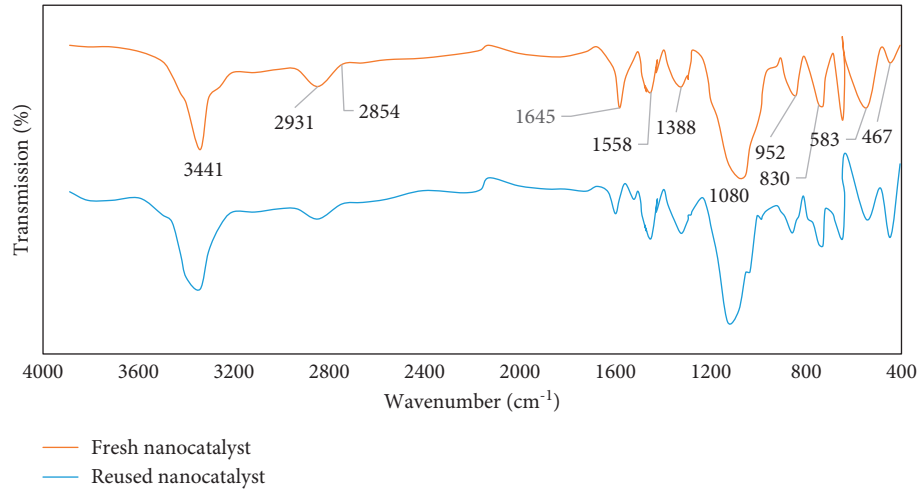

FIGURE 14: FT-IR spectrum of fresh and used [Fe_3O_4@SiO_2-NH_2-$Cu_{20}P_8W_{48}$] after eight cycles in the reduction of 4-NP.

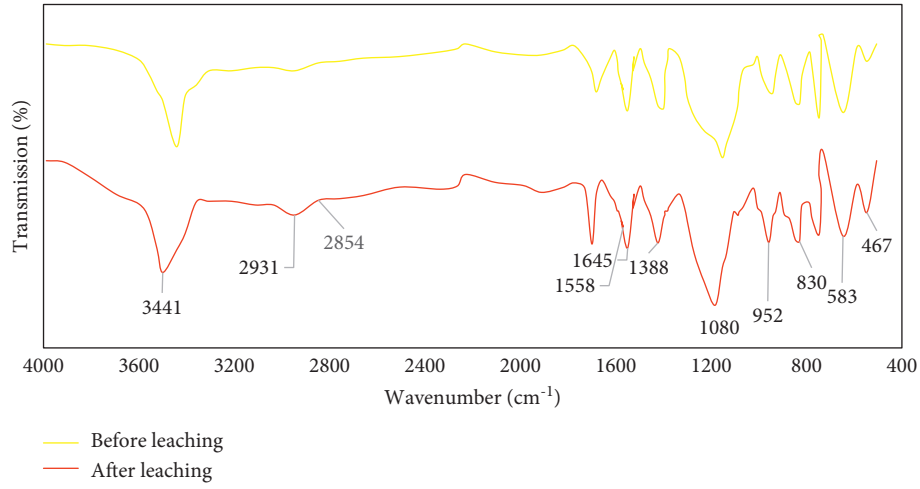

FIGURE 15: FT-IR spectra of after and before leaching.

3.2. Optimization of the Reaction Conditions. The comparison of the efficiency of the presence or absence of [Fe_3O_4@SiO_2-NH_2-$Cu_{20}P_8W_{48}$] nanocatalyst and also the effect of [Fe_3O_4], [Fe_3O_4@SiO_2], and [Fe_3O_4@SiO_2-NH_2] on the reduction efficiency of 4-NP have been investigated, and the results indicate the presence of $[Cu_{20}Cl(OH)_{24}(H_2O)_{12}(P_8W_{48}O_{184})]^{25-}$ was required (Figure 6). The higher catalytic activity of [Fe_3O_4@SiO_2-NH_2-$Cu_{20}P_8W_{48}$] compared to $[Cu_{20}Cl(OH)_{24}(H_2O)_{12}(P_8W_{48}O_{184})]^{25-}$, [$Fe_3O_4$], [$Fe_3O_4$@$SiO_2$], and [$Fe_3O_4$@$SiO_2$-$NH_2$] was related to the synergistic effect of [Fe_3O_4] NPs as a catalyst retainer, which plays an essential role in the structure of the catalyst by preventing the self-aggregation of $[Cu_{20}Cl(OH)_{24}(H_2O)_{12}(P_8W_{48}O_{184})]^{25-}$. Comparison of catalytic activity of $[Cu_{20}Cl(OH)_{24}(H_2O)_{12}(P_8W_{48}O_{184})]^{25-}$ with [Fe_3O_4@SiO_2-NH_2-$Cu_{20}P_8W_{48}$] shows lower conversion of $[Cu_{20}Cl(OH)_{24}(H_2O)_{12}(P_8W_{48}O_{184})]^{25-}$ even in longer times. This confirms the positive effect of [Fe_3O_4@SiO_2-NH_2] on the catalytic reduction process due to their large surface area.

3.2.1. Investigating the Effect of the Amount of Nanocatalyst and Reducing Agent. To obtain the most suitable amount of nanocatalyst and reducing agent required in the reduction of 4-NP, different amounts of [Fe_3O_4@SiO_2-NH_2-$Cu_{20}P_8W_{48}$] and $NaBH_4$ were investigated. The best reaction conditions were obtained with 0.01 g [Fe_3O_4@SiO_2-NH_2-$Cu_{20}P_8W_{48}$] and 200 mM $NaBH_4$ after 10 min (Figures 7 and 8).

3.2.2. Investigating the Effect of Temperature and Time. The effect of temperature in this catalytic system on the reduction of 4-NP was investigated. The results in Figure 9 clearly show that increasing the temperature does not affect on the rate of the reduction reaction.

3.3. Catalytic Reduction of 4-NP and 2,4,6,-TNP. The aqueous solution containing 4-NP displays a maximum absorption at 320 nm in a UV-Vis spectrum. After addition of $NaBH_4$, the characteristic peak assigned to 4-NP shifts from 320 nm to 400 nm due to the formation of 4-nitrophenolate anion (color change from light yellow to dark yellow). After the $[Fe_3O_4@SiO_2\text{-}NH_2\text{-}Cu_{20}P_8W_{48}]$, nanocatalysts were introduced into the system, and the absorption intensity of 4-NP at 400 nm rapidly decreases with time prolonged, accompanying by the appearance of the peak of 4-AP at 297 nm (Figure 10). In the absence of $[Fe_3O_4@SiO_2\text{-}NH_2\text{-}Cu_{20}P_8W_{48}]$, the 4-NP reduction does not take place even after a long time, which indicates the essential role of the $[Fe_3O_4@SiO_2\text{-}NH_2\text{-}Cu_{20}P_8W_{48}]$ in the catalytic reduction process.

The UV-Vis spectrum of 2,4,6,-TNP is similar to that of 4-NP, except that before the addition of $NaBH_4$, the peak in 354 nm is related to 2,4,6,-TNP, but after the addition of $NaBH_4$, a new peak appears in 391 nm due to the anion of 2,4,6,-TNP (color change from yellow to red). After adding $[Fe_3O_4@SiO_2\text{-}NH_2\text{-}Cu_{20}P_8W_{48}]$, peak at 391 nm was gradually removed and a new peak at 304 nm due to 2,4,6-TAP formation appeared (Figure 11).

3.4. Investigating the Possibility of Reusing Nanocatalyst $[Fe_3O_4@SiO_2\text{-}NH_2\text{-}Cu_{20}P_8W_{48}]$. The reusability of the $[Fe_3O_4@SiO_2\text{-}NH_2\text{-}Cu_{20}P_8W_{48}]$ was studied by using the nanocatalyst in recycling experiments. In order to regenerate the nanocatalyst, after 10 min of reaction, it was separated by using an external magnetic field, washed several times with distilled water and ethanol, and dried at 80°C for 2 h. It was then used in the reaction with a fresh reaction mixture. After six consecutive cycles, 100% selectivity and 2% reduction in conversion were observed (Figure 12). These results were investigated and confirmed using the UV-Vis spectrum (Figure 13). According to the UV-Vis spectrum, after the eighth cycle, a minimal peak is observed in the 400 nm region related to the 4-nitrophenolate anion. To evaluate the stability of $[Fe_3O_4@SiO_2\text{-}NH_2\text{-}Cu_{20}P_8W_{48}]$ in the reaction of reduction 4-NP and 2,4,6,-TNP after the eighth cycle, the nanocatalyst was separated using an external magnetic field after washing was examined for stability by the FT-IR spectrum. The results showed that the FT-IR spectrum did not change after the reaction compared to before the reaction, indicating an excellent electrostatic interaction between $[Cu_{20}P_8W_{48}]$ and NH_3^+ groups of $[Fe_3O_4@SiO_2\text{-}NH_2]$, which prevents leaching and separation of the nanocatalyst is deposited from the substrate surface and confirms the high stability of the nanocatalyst (Figure 14).

3.5. Leaching Studies. Necessary studies were performed to ensure that the principal elements and components of the $[Fe_3O_4@SiO_2\text{-}NH_2\text{-}Cu_{20}P_8W_{48}]$ did not separate from the surface of the $[Fe_3O_4@SiO_2\text{-}NH_2]$ substrate using the leaching test. First, $[Fe_3O_4@SiO_2\text{-}NH_2\text{-}Cu_{20}P_8W_{48}]$ nanocatalyst was immersed in water for 60 h, and then, the FT-IR spectra of the original nanocatalyst and nanocatalysts immersed in water were recorded and compared (Figure 15). The results show a good interaction between the nanocatalyst and the magnetic substrate.

3.6. The Proposed Mechanism for Hydrogenation of 4-NP and 2,4,6-TNP. The 4-NP and 2,4,6-TNP reduction mechanism consists of the following two steps: (1) absorption of $NaBH_4$ and nitrophenol compounds on the surface of $[Fe_3O_4@SiO_2\text{-}NH_2\text{-}Cu_{20}P_8W_{48}]$ and (2) electron transfer from BH_4^- to 4-NP and 2,4,6-TNP by catalytic reactions and then separate 4-AP and 2,4,6-TAP from the nanocatalyst surface (Scheme 2). An aqueous solution of 4-NP and 2,4,6-TNP in the presence of $NaBH_4$ leads to deprotonation of 4-NP and 2,4,6-TNP to nitrophenolate anions. In the second stage, the hydroxylamine(4-HO-(NO) phenyl (OH) intermediate with the continuous flow of electrons due to excess $NaBH_4$ is formed by the reduction of the nitro group to the amine. The surface of the nanocatalyst acts as a Lewis acid and absorbs electron pairs on the nitro group in nitrophenol compounds. According to reference [23], the $[Fe_3O_4@SiO_2\text{-}NH_2\text{-}Cu_{20}P_8W_{48}]$ nanocatalyst showed a very strong acidity of about 594 mV, while the $[Fe_3O_4@SiO_2]$ showed a weak acidity of about −67 mV due to silanol groups on the surface. The strong acidity of $[Fe_3O_4@SiO_2\text{-}NH_2\text{-}Cu_{20}P_8W_{48}]$ nanocatalysts is due to the presence of $[Cu_{20}P_8W_{48}]$, which increases the number and strength of acidic nanocatalyst sites.

4. Conclusions

In this study, an economical and environmentally friendly method for the reduction of nitrophenol compounds such as 4-NP and 2,4,6-TNP to aminophenol compounds using $[Fe_3O_4@SiO_2\text{-}NH_2\text{-}Cu_{20}P_8W_{48}]$ nanocatalyst in the presence of $NaBH_4$ was reported. The results showed that $[Fe_3O_4@SiO_2\text{-}NH_2\text{-}Cu_{20}P_8W_{48}]$ has a 100% conversion and selectivity in the reduction of nitrophenol compounds after 10 min under mild reaction conditions (e.g., in an aqueous solution at room temperature). The reuse of nanocatalyst up to eight cycles showed that only after the sixth cycle 2% reduction in efficiency is observed. After separating the nanocatalyst and washing it with water and ethanol, and drying it in vacuum, the FT-IR spectrum was investigated to evaluate the nanocatalyst stability before and after the reaction. Examination of the FT-IR spectrum after the eighth step showed precisely the same results as the pre-reaction spectrum, which indicates the high stability of the nanocatalyst after the reaction.

Data Availability

The data used to support the findings of this study are available from the author upon request.

Conflicts of Interest

The authors declare that there are no conflicts of interest.

Acknowledgments

The authors wish to thank the Research Council of the Policing Sciences and Social Studies Institute, which is highly appreciated.

References

[1] C. Karaman, O. Karaman, N. Atar, and L. M. Yola, "Electrochemical immunosensor development based on core-shell high-crystalline graphitic carbon nitride@carbon dots and Cd0.5Zn0.5S/d-Ti3C2Tx MXene composite for heart-type fatty acid–binding protein detection," *Microchimica Acta*, vol. 188, 2021.

[2] F. A. Beni, A. Gholami, A. Ayati, M. N. Shahrak, and M. Sillanpaa, "UV-switchable phosphotungstic acid sandwiched between ZIF-8 and Au nanoparticles to improve simultaneous adsorption and UV light photocatalysis toward tetracycline degradation," *Microporous and Mesoporous Materials*, vol. 303, 2020.

[3] D. Van-Dat, L. P. Thanh, T. L. Van et al., "Efficient and fast degradation of 4-nitrophenol and detection of Fe(III) ions by *Poria cocos* extract stabilized silver nanoparticles," *Chemosphere*, vol. 286, Article ID 131894, 2022.

[4] M. E. Mahmoud, M. F. Amira, M. E. Abouelanwar, and S. M. Seleim, "Catalytic reduction of nitrophenols by a novel assembled nanocatalyst based on zerovalent copper-nano-polyaniline-nanozirconium silicate," *Journal of Molecular Liquids*, vol. 299, Article ID 112192, 2020.

[5] H. Karimi-Maleh, M. Shafieizadeh, M. A. Taher et al., "The role of magnetite/graphene oxide nano-composite as a high-efficiency adsorbent for removal of phenazopyridine residues from water samples, an experimental/theoretical investigation," *Journal of Molecular Liquids*, vol. 298, Article ID 112040, 2020.

[6] V. T. Le, V.-C. Nguyen, X.-T. Cao et al., "Highly effective degradation of nitrophenols by biometal nanoparticles synthesized using *Caulis spatholobi* extract," *Journal of Nanomaterials*, vol. 2021, Article ID 6696995, 11 pages, 2021.

[7] L. MacDonald, B. Rausch, M. D. Symes, and L. Cronin, "Selective hydrogenation of nitroarenes using an electrogenerated polyoxometalate redox mediator," *Chemical Communications*, vol. 54, no. 9, pp. 1093–1096, 2018.

[8] Y. Gao, M. Tian, Y. Jia, X. Wang, and L. Yang, "Polyoxometalates as catalysts for fluorescence amplification in rapid and sensitive detection of artemisinin," *Analytica Chimica Acta*, vol. 1143, pp. 101–108, 2021.

[9] J. Du, Y.-Y. Ma, H. Tan, Z.-H. Kang, and Y. Li, "Progress of electrochemical CO_2 reduction reactions over polyoxometalate-based materials," *Chinese Journal of Catalysis*, vol. 42, no. 6, pp. 920–937, 2021.

[10] S. Wang, X. Wang, X.-Y. Shi, C.-X. Meng, C.-L. Sun, and Z.-S. Wu, "A three-dimensional polyoxometalate/graphene aerogel as a highly efficient and recyclable absorbent for oil/water separation," *New Carbon Materials*, vol. 36, no. 1, pp. 189–197, 2021.

[11] R. Wang, X. Zhang, and Z. Ren, "Germanium-based polyoxometalates for the adsorption-decomposition of NOx," *Journal of Hazardous Materials*, vol. 402, Article ID 123494, 2021.

[12] X. Xin, N. Hu, Y. Ma et al., "Polyoxometalate-based crystalline materials as a highly sensitive electrochemical sensor for detecting trace Cr(vi)," *Dalton Transactions*, vol. 49, no. 14, pp. 4570–4577, 2020.

[13] G. Liu, T. Liu, S. S. Mal, and U. Kortz, "Wheel-shaped polyoxotungstate $[Cu_{20}Cl(OH)_{24}(H2O)_{12}(P_8W_{48}O_{184})]^{25-}$ macroanions form supramolecular "blackberry" structure in aqueous solution," *Journal of the American Chemical Society*, vol. 128, no. 31, pp. 10103–10110, 2006.

[14] S. D. Ovhal, C. S. Rodrigues, and L. M. Madeira, "Photocatalytic wet peroxide assisted degradation of orange II dye by reduced graphene oxide and zeolites," *Journal of Chemical Technology and Biotechnology*, vol. 96, no. 2, pp. 349–359, 2021.

[15] A. Ucar, M. Findik, I. H. Gubbuk, N. Kocak, and H. Bingol, "Catalytic degradation of organic dye using reduced graphene oxide-polyoxometalate nanocomposite," *Materials Chemistry and Physics*, vol. 196, pp. 21–28, 2017.

[16] L. Wang, W. Fu, Y. Zhuge et al., "Synthesis of polyoxometalates (POM)/TiO_2/Cu and removal of nitrate nitrogen in water by photocatalysis," *Chemosphere*, vol. 278, Article ID 130298, 2021.

[17] N. M. Mahmoodi, M. A. Rezvani, M. Oveisi, A. Valipour, and M. A. Asli, "Immobilized polyoxometalate onto the modified magnetic nanoparticle as a photocatalyst for dye degradation," *Materials Research Bulletin*, vol. 84, pp. 422–428, 2016.

[18] S. Rana and K. M. Parida, "A simple and efficient protocol using palladium based lacunary phosphotungstate supported mesoporous silica towards hydrogenation of p-nitrophenol to p-aminophenol at room temperature," *Catalysis Science and Technology*, vol. 2, no. 5, pp. 979–986, 2012.

[19] D.-Y. Du, J.-S. Qin, C.-G. Wang et al., "Redox-active polyoxometalate-based crystalline material-immobilized noble metal nanoparticles: spontaneous reduction and synergistic catalytic activity," *Journal of Materials Chemistry*, vol. 22, no. 39, pp. 21040–21044, 2012.

[20] H.-l. Li, N. Perkas, Q.-l. Li, Y. Gofer, Y. Koltypin, and A. Gedanken, "Improved silanization modification of a silica surface and its application to the preparation of a silica-supported polyoxometalate catalyst," *Langmuir*, vol. 19, no. 24, pp. 10409–10413, 2003.

[21] M. Kamada, H. Kominami, and Y. Kera, "Deposition and interaction of phosphododecatungstate on a silica gel surface modified with a silane coupling agent having anilino groups," *Journal of Colloid and Interface Science*, vol. 182, no. 1, pp. 297–300, 1996.

[22] S. S. Mal and U. Kortz, "The wheel-shaped Cu_{20} tungstophosphate $[Cu_{20}Cl(OH)_{24}(H2O)_{12}(P_8W_{48}O_{184})]^{25-}$ ion," *Angewandte Chemie International Edition*, vol. 44, no. 24, pp. 3777–3780, 2005.

[23] R. Haddad, M. D. Telgerd, H. Abedi, and A. Roostaie, "Nano-polyoxotungstate as a recyclable and highly efficient catalyst for cycloaddition of CO_2 to cyclic carbonates under solvent-free conditions," *Current Organic Synthesis*, vol. 15, no. 4, pp. 533–540, 2018.